Contents lists available at ScienceDirect

Biosensors and Bioelectronics

journal homepage: www.elsevier.com/locate/bios

A novel electrochemical imprinted sensor for ultrasensitive detection of the new psychoactive substance "Mephedrone"

Iman Razavipanah[a,*], Esmaeel Alipour[b], Behjat Deiminiat[a], Gholam Hossein Rounaghi[a]

[a] *Department of Chemistry, Faculty of Sciences, Ferdowsi University of Mashhad, Mashhad, Iran*
[b] *Department of Analytical Chemistry, Faculty of Chemistry, University of Tabriz, Tabriz, Iran*

A B S T R A C T

Identification and quantitation of mephedrone as one of the popular new psychoactive substances (NPSs) in biological fluids is important. In this study, a novel electrochemical imprinted sensor was designed for ultrasensitive and selective measurement of mephedrone, based on sol-gel molecular imprinted polymer, polytyramine and functionalized multi-walled carbon nanotube@ gold nanoparticles (f-MWCNT@AuNPs) nanocomposite. The developed electrochemical sensor inherits characteristics of the gold and MWCNTs such as high electrical conductivity, large specific surface area and good biocompatibility. Also, tyramine as an additional monomer was used for fabrication of a strongly adhering film on the surface of the electrode. In the proposed method, the concentration of mephedrone was determined indirectly. The change in the current response of $[Fe(CN)_6]^{3-/4-}$ redox probe in the presence and absence of mephedrone molecules was used for indirect measurement of mephedrone molecule in solution. Density functional theory (DFT) was applied to better understanding the interactions between the mephedrone, sol-gel polymer and tyramine from molecular viewpoint. Under the optimized experimental conditions, the calibration curve of the designed sensor was plotted and two dynamic linear ranges from 1 to 10 nM and 10–100 nM with a limit of detection (LOD) as low as 0.8 nM (142 pg ml^{-1}) were obtained. Finally, the fabricated sensor was successfully used to detect the mephedrone in biological samples.

1. Introduction

New psychoactive substances (NPSs), known as "legal highs" have effects like traditional drug of abuse (Smith et al., 2014). These compounds are defined as NPSs because, they are not prohibited by United Nations Drug Conventions of 1961 and 1971, or by Misuse of Drugs Act 1971. Nevertheless, NPSs may pose a public health threat similar to those listed in these conventions (Advisory Council on the Misuse of Drugs, 2015). Mephedrone is one of the popular NPSs which provide effects like amphetamines and cocaine. Widespread use of this substance is of particular concern due to its negative health implication such as chest pain, sweating, blurred vision, agitation, brief psychosis, and hypertension on bodies (Wood et al., 2011).

Now a day, different analytical methods such as gas chromatography-mass spectrometry (GC-MS), high performance liquid chromatography (HPLC), liquid chromatography-tandem mass spectrometry (LC-MS/MS) and tandem mass spectrometry (MS-MS) have been developed for detection of mephedrone (Torrance and Cooper, 2010; Santali et al., 2011; Jankovics et al., 2011; Lua et al., 2012). However,

these methods are time consuming, expensive and require expert operators and sophisticated instruments. On the other hand, electrochemical methods are simple, sensitive and far less expensive than the aforementioned techniques (Zhou et al., 2018; Qiu et al., 2018; Zhang et al., 2018; Shu and Tang, 2017; Zhang et al., 2017).

Molecular imprinting is a powerful technique which is widely used for preparation of polymeric material for molecular recognition (Haupt and Mosbach, 2000; Wang et al., 2003; Mohamed et al., 2007). Molecular imprinted polymer (MIP) strategy has been extensively used in preparation of various chemical sensors due to low cost, ease of preparation and high selectivity of MIP method (Deiminiat et al., 2017a; Yuan et al., 2011). Nevertheless, the traditional MIP strategy has suffered from a series of limitations such as long response time, limited surface area, heterogeneous nature of the binding sites and slow diffusion of the target from the binding sites (Rezaei et al., 2014). Therefore, some new approaches have been developed for preparation of imprinting films (Prasad and Singh, 2015; Madrakian et al., 2015; Sun et al., 2016). The sol-gel imprinting is one such progression. Compare to the conventional MIP technology, sol-gel MIP has some

prominent advantages including, high porosity, thermal stability, ease of preparation, mild reaction condition and good physical rigidity (Yang et al., 2013; Zhang et al., 2014). The combination of the molecular imprinting with the sol-gel strategy, is proper idea to construct the chemical sensors.

Recently, the composite materials based on the coupling of the metal nanoparticles and CNTs with the goal of improving the electrochemical and mechanical properties, which are not observed in the individual components, have been widely used for development of various sensor (Bagheri et al., 2017; Gao et al., 2007). A nanocomposite of CNTs and gold nanoparticles is of great interest due to the desirable merging of properties of CNTs such as large surface area, high electrical conductivity and chemical stability together with good biocompatibility and unique electronic and optical properties of the gold nanoparticles which leads to a superior performance of the resulting sensing devices (Hamidi et al., 2017; Afkhami et al., 2016).

In the recent years, tyramine (Ty), 4-(2-aminoethyl) phenol, as one of the phenol derivatives has been applied for development of biosensors (Miscoria et al., 2006; Wu et al., 2005). It can be easily electropolymerized through its phenol moiety and fabricate an adhering film on the surface of electrode (Tran et al., 2003; Situmorang et al., 1998).

In the present work, an electrochemical MIP sensor was designed for the first time for detection of mephedrone based on sol-gel MIP technology, polytyramine and f-MWCNT@AuNPs nanocomposite. The combination of these materials, results in construction of a new sensor with high analytical performance capabilities for quantitative measurement of mephedrone in solutions.

2. Experimental

2.1. Materials

Mephedrone was kindly donated by the Research Center of Antinarcotic Police (Tehran, Iran). Tetraethoxysilane (TEOS), phenyltriethoxysilane (PTEOS), trifluoroaceticacid (TFA), sodium dodecyl sulfate (SDS) and tetrakis (hydroxymethyl) phosphonium chloride (THPC) were purchased from Merck chemical company (Darmstadt, Germany) and tyramine was obtained from Acros (New Jersey, USA). MWCNTs (purity > 95%, length range 5–15 µm, specific surface area > 40–300 $m^2 g^{-1}$) were purchased from Shenzhen Nanotech Port (Shenzhen, China). Hydrogen tetrachloroaurate trihydrate (HAuCl$_4$·3H$_2$O) was supplied from Sigma-Aldrich (USA). All of the solvents and the other salts used in this study, were of analytical grade and were obtained from Merck (Darmstadt, Germany).

2.2. Synthesize of f-MWCNT@AuNPs nanocomposite

The f-MWCNT@AuNPs nanocomposite was synthesized according to our previous report (Deiminiat et al., 2017b). The procedure for synthesize of the nanocomposite, has been described in detail in the Supporting information.

2.3. Development of sol-gel MIP/polytyramine/f-MWCNT@AuNPs nanocomposite/GCE

The sol solution was obtained by mixing 75 µL PTEOS, 75 µL TEOS, 700 µL H$_2$O, 1100 µL EtOH, 10 µL of TFA and mephedrone (2.0 mM) in a vial and it was stirred for 2 h. Then, 8.0 mg tyramine, 5.0 mg SDS and 50 µL of f-MWCNT@AuNPs nanocomposite (1 mg ml^{-1} in DMF) were added to the homogeneous sol solution. The resulting solution was sonicated for 10 min. Next, the GC electrode was immersed into the sol solution. The MIP film was deposited on the surface of the electrode using cyclic voltammetry at the potential range between − 0.8 and 1.2 V vs. Ag/AgCl at scan rate of 50 mV s^{-1}. The modified GCE was dried at room temperature for 2 h and subsequently immersed in

methanol-acetic acid (9:1, v/v) solution for 20 min, to remove the template from the polymeric matrix. A non-imprinted polymer (NIP) electrode was also fabricated under the same experimental conditions without the presence of the template molecule in the solution.

3. Results and discussion

### 3.1. Detection principle and measurement process of the MIP sensor

Detection principle is based on this fact that template removal from the polymer film creates some cavities in it. These cavities facilitate the diffusion of active probe through the imprinted polymer to the electrode surface. Therefore, the concentration of mephedrone can be determined indirectly, by measuring the intensity of the electrochemical signal of a redox probe. Since, mephedrone is not an electroactive compound over the studied potential range, [Fe(CN)$_6$]$^{3-/4-}$ was chosen as the redox probe in the determination procedure. The electrochemical measurements were carried out in a probe solution containing 0.1 M KCl and 5.0 mM [Fe(CN)$_6$]$^{3-/4-}$ redox pair. In each experiment, at first the current response of [Fe(CN)$_6$]$^{3-/4-}$ redox probe was measured. Then, the sensor was incubated in mephedrone solution and again the corresponding current of [Fe(CN)$_6$]$^{3-/4-}$ redox probe was recorded. It should be mentioned that when the MIP electrode is immersed in the mephedrone solution, the mephedrone molecules occupy the binding cavities in the imprinted film, which leads to decrease the probe current response (Scheme S1). By increasing the concentration of the mephedrone, more imprinted cavities are occupied and thus, the current response further decreases. The change in the current response of [Fe(CN)$_6$]$^{3-/4-}$ redox probe (Δi_p) was applied for quantitative measurement of mephedrone in solutions. Δi_p, was calculated by subtracting the current which was obtained in the absence of mephedrone from the current recorded in the presence of mephedrone molecules.

3.2. Characterization of the synthesized f-MWCNT@AuNPs nanocomposite and molecular imprinted sensor

It has been shown that the high surface energy of the Au nanoparticles with diameter in low nanometer range often leads to their aggregation (Zhao et al., 1998). One approach to overcome this problem, is the immobilization of the gold nanoparticles on the solid supports (Shen et al., 2011; Donkova et al., 2011). In order to prevent the aggregation of the Au nanoparticles, we used f-MWCNTs as a solid support. Fig. 1A, exhibits the TEM image of a single strand carbon nanotube in the presence of Au nanoparticles. As is evident in this Figure, the AuNPs have been successfully attached on the surface of the f-MWCNT single strand. A careful inspection of this Figure confirms that Au nanoparticles have no tendency to aggregate on this surface. Fig. 1B, shows a typical EDX of the f-MWCNTs@AuNPs nanocomposite. The Au peaks which are clearly seen in this Figure, reveals that the AuNPs are adsorbed on the surface of functionalized multi-walled carbon nanotubes.

In order to support the TEM and EDX findings, the XRD patterns of the f-MWCNT and f-MWCNT@AuNPs nanocomposite were also recorded. Fig. 1C, shows the crystalline structure of the f-MWCNT@AuNPs nanocomposite. The presence of the dominant crystal growth planes of (111) compare to the XRD pattern of f-MWCNT, confirms the stabilization of the gold nanoparticles on the surface of the f-MWCNTs.

The surface morphology of the nanocomposite film was also investigated by SEM technique. Comparison of the SEM image of bare GCE surface (Fig. 1D) with the SEM image of the nanocomposite (Fig. 1E), confirms that a uniform layer of the sol-gel MIP/polytyramine/f-MWCNT@AuNPs film has been attached on the surface of the GCE. To further evaluate the existence of the sol-gel MIP/polytyramine/f-MWCNT@AuNPs film on the surface of glassy carbon electrode, EDX technique was also employed. The results obtained from
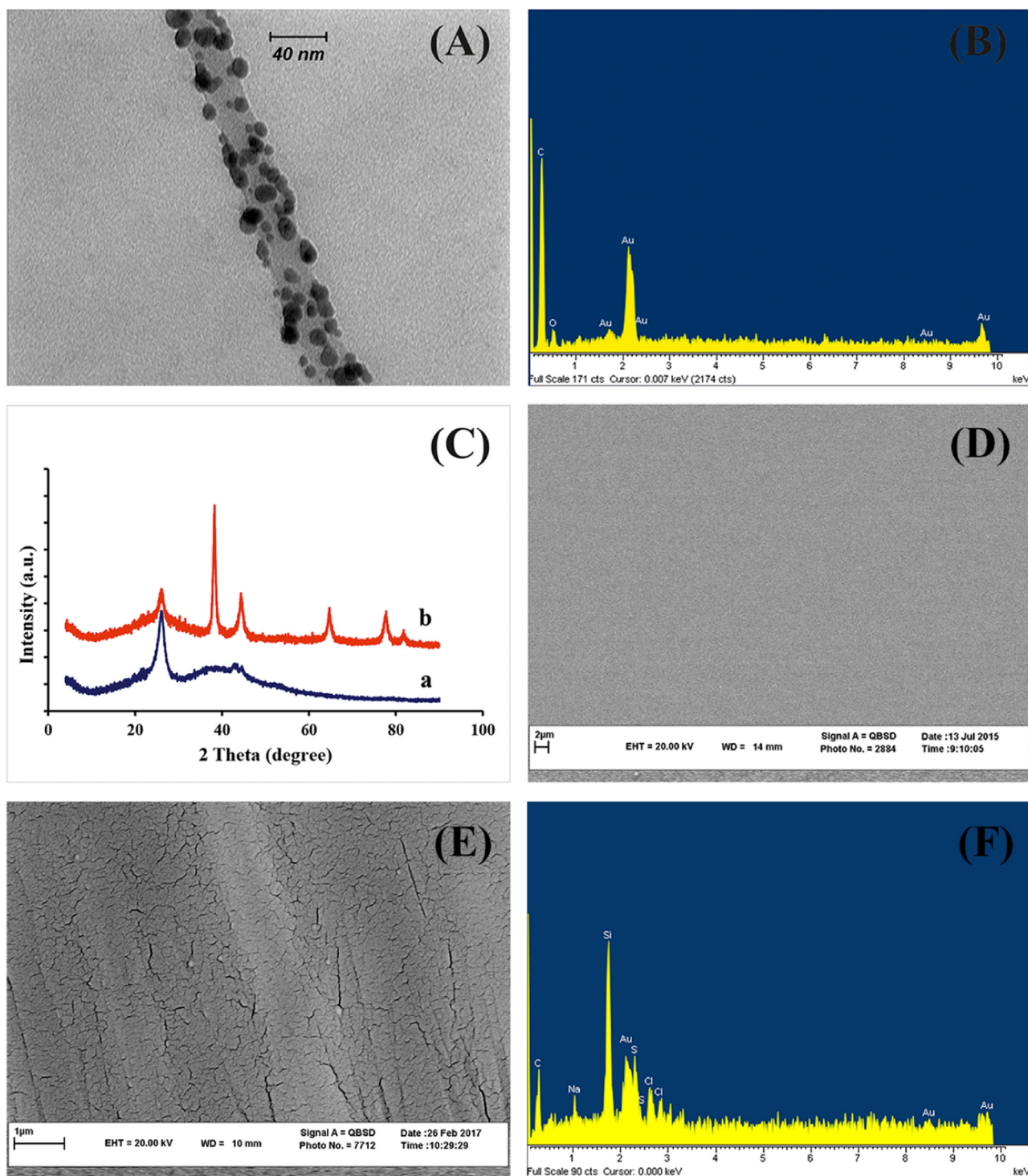
Fig. 1. A) TEM image of f-MWCNTs@AuNPs nanocomposite. B) EDX analysis results for f-MWCNTs@AuNPs nanocomposite. C) XRD patterns of (a) f-MWCNTs, (b) f-MWCNTs@AuNPs nanocomposite. D) SEM image of bare GCE. E) SEM image of sol-gel MIP/polytyramine/f-MWCNT@AuNPs film. F) EDX analysis results for sol-gel MIP/polytyramine/f-MWCNT@AuNPs film.

EDX analysis (Fig. 1F), show that a polymer film is formed on the surface of the GCE.

3.3. Electrochemical characterization of imprinted sensor

Cyclic voltammetric (CV) measurements were carried out to characterize the electrochemical properties of sensor at different modification steps. Fig. 2, shows the CV profiles of the bare and modified electrodes in the presence of $[Fe(CN)_6]^{3-/4-}$ redox probe. Curve a, shows

the electrochemical signal which belongs to the redox probe at the surface of the bare GCE. When the polymer film is electrodeposited on the surface of the GCE, the intensity of the electrochemical signal decreases significantly, because the $[Fe(CN)_6]^{3-/4-}$ anions cannot reach to the electrode surface and therefore, the electron transfer carries out with difficulty. This behavior indicates the formation of MIP film on the surface of the electrode (curve b). When, the template molecules are removed from the MIP matrix, the intensity of the electrochemical signal increases which shows that the redox probe molecules can reach
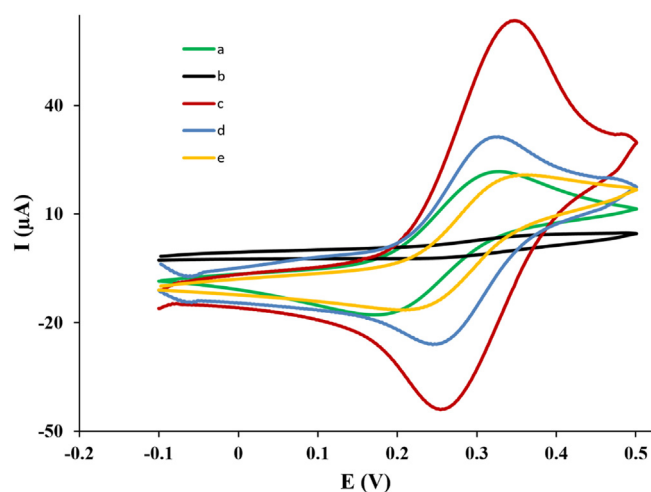
Fig. 2. Proof of concept for the fabricated MIP sensor. Cyclic voltammograms of (a) bare GCE, (b) sol-gel MIP/polytyramine/f-MWCNT@AuNPs/GCE, (c) sol-gel MIP/polytyramine/f-MWCNT@AuNPs/GCE after removal of mephedrone, (d) sol-gel MIP/polytyramine/f-MWCNT@AuNPs/GCE after 420 s incubation in 20 nM mephedrone solution, (e) sol-gel MIP/polytyramine/GCE after removal of mephedrone. Conditions: Potential scan range − 0.1 V to + 0.5 V, Scan rate 50 mV s^{-1}.

easily to the electrode surface through the established cavities (curve c). After incubation of the sol-gel MIP/polytyramine/f-MWCNT@AuNPs/ GCE in 20 nM mephedrone solution, the intensity of the electrochemical signal reduces. It seems that after incubation of the electrode in mephedrone sample solution for a specific time, some of the cavities are recombined with the mephedrone molecules which limits the chance of the redox probe to electron exchange with the electrode surface (carve d). In order to evaluate the role of the f-MWCNT@AuNPs nanocomposite on the intensity of the electrochemical signal of the proposed sensor, the CV profile of the modified electrode in the absence of the f-MWCNT@AuNPs nanocomposite was recorded. As can be seen in curve e, the current response of the electrode decreases compared to the cyclic voltammogram which is obtained for the sol-gel MIP/polytyramine/f-MWCNT@AuNPs glassy carbon electrode. This behavior shows that the presence of f-MWCNT@AuNPs nanocomposite in the polymer matrix, facilitates the electron transfer process which may be due to the high conductivity and large surface area of the nanocomposite.

3.4. Quantum calculation studies

The optimized structures of mephedrone, sol-gel MIP, tyramine and also the mephedrone complexes with sol-gel MIP and tyramine are shown in Fig. 3A. The calculated values of the Gibbs free energies for the interactions between mephedrone-tyramine and mephedrone-sol-gel MIP are − 19.58 and − 4.46 kJ mol^{-1}, respectively. The values of the Gibbs free energies, indicate that the mephedrone molecules, have a stronger interaction with tyramine molecule compared to the sol-gel MIP. Fig. 3B, shows the molecular graphs of the mephedrone complexes with the sol-gel MIP and tyramine. The quantum theory of atoms in molecules (QTAIM) analysis was applied to better understanding the interactions between the mephedrone, tyramine and the sol-gel MIP. The resulted topological parameters are summarized in Table S1. As is evident in Table S1, the bond strength increases with increasing the electron density (ρ). The obtained results reveal that the calculated value of ρ for the H48….N23 bond of the mephedrone-tyramine interaction is bigger than that of the O11….H43 bond. Moreover, the calculated electron density of the H15….O26, H6….O26 and H39….O10 bonds of the mephedrone-sol-gel MIP complex are 0.025, 0.028 and 0.010, respectively. These results indicate that the mephedrone
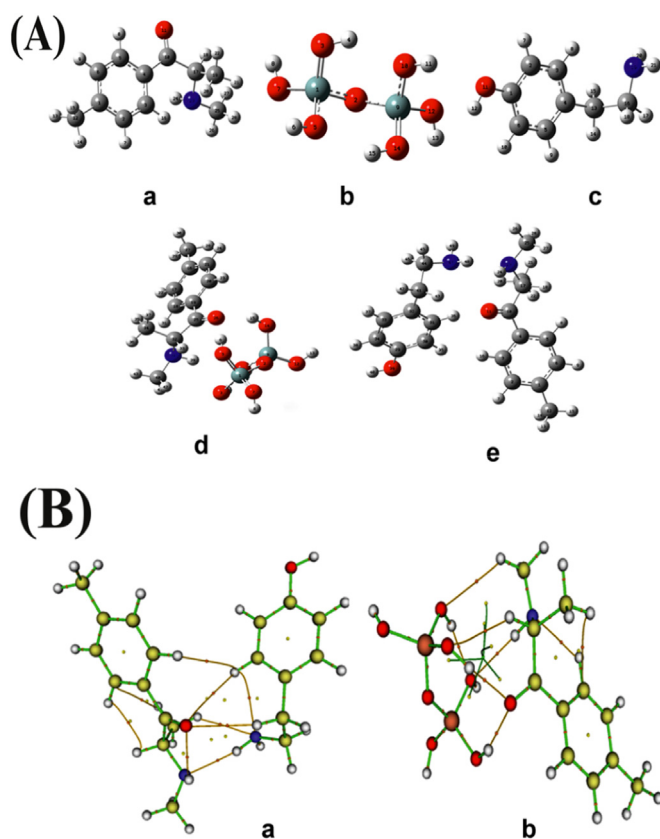
Fig. 3. A) Optimized structures of (a) mephedrone, (b) sol-gel, (c) tyramine, (d) mephedrone-sol-gel, e) mephedrone-tyramine at the B3LYP/6–31G(d) level. B) Molecular graphs of the mephedrone complexes with (a) tyramine, (b) sol-gel MIP at the B3LYP/6–31G(d) level.

molecule has a stronger electrostatic interaction with sol-gel MIP compared to the tyramine monomers.

The calculated positive Laplacian (L(r)) values for all bonds which show an electrostatic interaction between the mephedrone molecule and the functional monomers, are listed in Table S1. The ratio of the kinetic energy density (G) to the potential energy density (V) at the bond critical points (BCP) of O….H and N….H bonds is near to 1.0 which is an evidence for an electrostatic interaction between the mephedrone molecules and the functional monomers.

3.5. Optimization of parameters affecting the sensor performance

In order to enhance the analytical performance of the fabricated electrochemical sensor, several key parameters including the number of scan cycles of electropolymerization process, pH of the mephedrone solution and incubation time were optimized.

3.5.1. Effect of the thickness of the polymer film

The electrochemical signal of the MIP sensor can be affected by the thickness of the polymer film because the thickness of the modifier can influence the mass transfer mechanism via diffusion through the porous film (Xiao et al., 2009; Banks et al., 2005; Banks and Compton, 2006). Hence, the number of scan cycles during the electropolymerization process must be investigated in order to obtain the optimum current response. For this purpose, the number of scan cycles was changed from 3 to 16 and the current responses were recorded. As is evident in Fig. S1, the current response increases with the number of the cycles from 3 to 10 and then decreases at higher number of scan cycles. The decrease in the current response for higher number of scan cycles, is due to the formation of a thick modifier film. The thick film, on one hand,

decreases the mass transfer process through the porous film and on the other hand, causes the less imprinting sites to be accessible for the mephedrone molecules (Lian et al., 2013).

3.5.2. Conditions of the sol solution

It is obvious that the composition of the modifier film, affects the performance of the sensor. For instance, the functional monomers such as TEOS and PTEOS have a principal role for optimizing the molecular imprinting process. TEOS is known as a cross-linker and used to form a polymer network around the template molecule via hydrogen bonds and ionic interactions. PTEOS, as a functional monomer was also used to create the л-л interactions with the aromatic ring of the template molecules (Deiminiat et al., 2017c). In this work, tyramine as an additional monomer was incorporated into the sol solution, in order to increase the stability of the resultant MIP matrix. Also, the free amine group of the tyramine can form hydrogen bond with the C=O group of the mephedrone molecule. Therefore, a series of sol-gel MIP/poly-tyramine/f-MWCNT@AuNPs electrodes were constructed by varying the amount of TEOS, PTEOS (in the range of the 100–300 μL) and tyramine concentration (in the range of the 5.0–50 mM). The optimum amounts of these functional monomers were found to be: 150 μL of silane monomers (75 μL TEOS and 75 μL of PTEOS) and 30 mM of tyramine monomer. It seems that under these conditions, optimum number of imprinted sites and film thickness are achieved on the surface of the electrode.

The effect of the amount of the template and f-MWCNT@AuNPs nanocomposite was also evaluated and experimental results, showed that 2 mM of the template and 2.5×10^{-3} percent (%W/V) of the f-MWCNT@AuNPs nanocomposite are the best values for fabrication of the MIP sensor.

3.5.3. Rebinding conditions

Selection of the best condition for incubation step is an effective way to enhance the sensitivity of MIP sensor. After removing the template molecule from the electrode surface, the imprinted electrode was incubated in 20 nM mephedrone solution for various period of time and the current response was recorded. Fig. S2, indicates the current response as a function of incubation time. As shown in this Figure, the current responses rose progressively with the time from 60 to 420 s and then, it becomes nearly constant. Thus, 420 s was selected as optimum time for incubation step, in the next experiments.

Also, the pH of the solution is an effective parameter on the template molecule rebinding. Therefore, the influence of the pH of the mephedrone solution was investigated on the electrochemical signal of the modified electrode. To this end, the pH of the mephedrone solution was changed between 4.0 and 10 and the current response was recorded. As is evident in Fig. S3, the maximum current response is obtained at pH 6.0. The obtained results indicate that the interaction between the template molecules and the binding sites is facilitated at this pH value.

3.6. Quantitative measurement of mephedrone in solution

Square wave voltammetry (SWV) technique was applied for measurement of mephedrone in solution. Fig. 4A, shows the SWV peaks of the designed electrode at different concentration of mephedrone. After removal of template and background signal measurements, the modified electrode was immersed in the mephedrone solution (with different concentration) and the corresponding redox peak currents were recorded. The proposed sensor displays two linear ranges from 1 to 10 and 10–100 nM toward mephedrone concentration (Fig. 4B). It seems that two linear concentration ranges of the sensor are due to the existence of different kinds of binding sites with diverse affinities toward the mephedrone molecules at the surface of MIP matrix (Li et al., 2016). The limit of detection (LOD) was found to be 0.8 nM (142 pg ml^{-1}) regarding the three times of the standard deviation of the blank divided
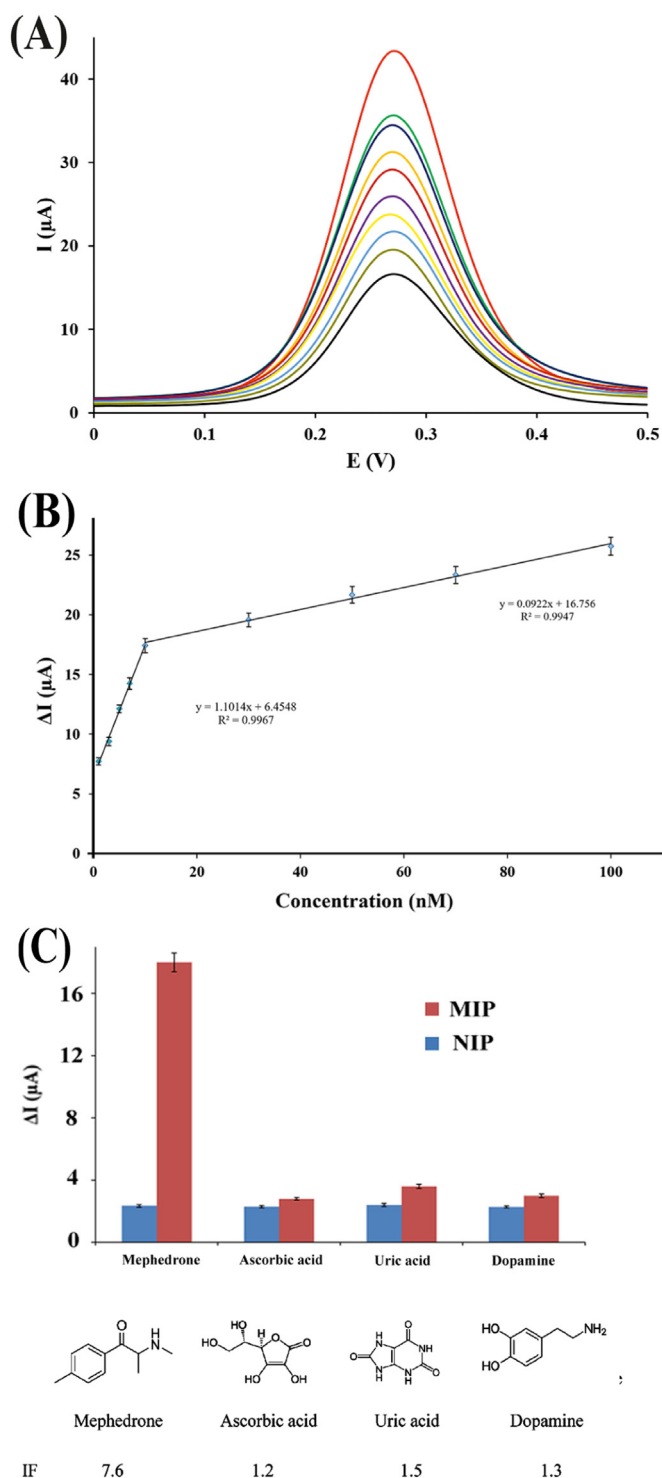

Fig. 4. A) Square wave voltammograms of sol-gel MIP/polytyramine/f-MWCNT@AuNPs/GCE at various concentrations of mephedrone in solution (from top to bottom 0, 1, 3, 5, 7, 10, 30, 50, 70 and 100 nM). B) Calibration curve of MIP sensor in mephedrone solution. Error bars represent the standard deviations for three replicate measurements. The numerical values for the relative standard deviations at each concentration are 3.9%, 3.6%, 2.7%, 3.5%, 3.4%, 2.9%, 3.2%, 3.0% and 2.9% from low concentration to high concentration, respectively. C) Selectivity of the imprinted and non-imprinted sensor for mephedrone and interferences. The numerical values for the relative standard deviation of MIP are 3.3%, 3.2%, 3.9% and 4%, and NIP are 3.4%, 3.0%, 4.2% and 3.1%.

Table 1
Comparison of the LOD of the proposed sensor with the other instrumental methods used for detection of mephedrone.

No.	Detection method	Limit of detection (LOD)	Ref.
1	HPLC-AD	82.7 nM	(Zuway et al., 2015)
2	UHPLC–MS-MS	5.6 nM	(Amaratunga et al., 2013)
3	Electrochemistry	3.2 nM	(Tan et al., 2015)
4	LC–MS-MS	17 nM	(Mercolini et al., 2016)
5	LC-MS-MS	0.3 nM	(Li et al., 2014)
6	SERS	9.1 μM	(Mabbott et al., 2013)
7	UHPLC–MS-MS	11.3 nM	(Johnson and Botch-Jones, 2013)
8	GC-MS	5.6 nM	(Meyer et al., 2010)
9	Electrochemistry	0.8 nM	This work

HPLC-AD: High performance liquid chromatography-amperometric detection.
UHPLC–MS-MS: Ultrahigh-performance liquid chromatography-tandem mass spectrometry.
LC–MS-MS: Liquid chromatography-tandem mass spectrometry.
SERS: Surface enhanced Raman scattering.
GC-MS: Gas chromatography-mass spectrometry.

by the slope of the calibration curve.

The value of LODs obtained by different methods for determination of mephedrone are summarized in Table 1. As is evident in this Table, the LOD of the fabricated electrochemical sensor, is lower than those obtained by the other experimental techniques which are expensive and also time consuming.

3.7. Evaluation of selectivity, repeatability, reproducibility and stability of the fabricated electrochemical imprinted sensor

An applicable electrochemical sensor must have a high selectivity toward a specific target and also, it should have a wide concentration range for its target with a low detection limit. Therefore, the effect of some of the probable interfering species existing in biological fluids such as ascorbic acid, dopamine and uric acid on determination of the mephedrone were studied and the corresponding results are given in Fig. 4C. A key parameter for investigation of the selectivity of the MIP sensor is imprinting factor, which is defined as the ratio of the Δi_{MIP} to the Δi_{NIP}. A careful inspection of the Fig. 4C, shows that the imprinting factor for mephedrone is 7.6. However, the value of this parameter for ascorbic acid, dopamine and uric acid are 1.2, 1.3 and 1.5, respectively. These experimental results, clearly confirm the higher selectivity of the proposed sensor toward the mephedrone molecules compare to the interfering species.

The precision of the electrochemical assays for measurement of the mephedrone in solution was evaluated by determination of the repeatability and the reproducibility of the method. The repeatability which is expressed as the relative standard deviation (RSD), was obtained by consecutive measurement of the mephedrone analyte with one of the fabricated imprinted sensor. For this purpose, the electrochemical response of a 20 nM mephedrone solution was measured sequentially for 14 times and the RSD was obtained 3.6. Likewise, in order to investigate the sensor-to-sensor reproducibility, five similarly constructed sensors, were tested under the optimum experimental conditions and the RSD was obtained 4.4. These findings show that the designed molecular imprinted sensor, has a good repeatability and reproducibility.

To investigate the stability of the sensor, it was stored at 4 °C in refrigerator for two weeks. Then, it was used for measurement of mephedrone every day for two weeks. The results obtained from these experiments indicate that the current response of the modified electrode retained 91.5% of its initial value after two weeks which confirms that the developed sensor has an acceptable stability.

Table 2
Results of mephedrone determination in real samples (n = 3).

Sample	Added (nM)	Detected (nM)	Recovery (%)	RSD (%)
Plasma	–	Not detected	–	–
	3.0	2.9	97	2.7
	5.0	4.8	96	3.1
	7.0	7.3	104	4.1
	10.0	10.7	107	4.7
Urine	–	Not detected	–	–
	3.0	2.9	97	3.1
	5.0	5.5	110	3.6
	7.0	7.4	106	4.4
	10.0	9. 8	98	4.0

3.8. Measurement of mephedrone in real samples

Although the fabricated sensor showed good figures of merit when using mephedrone standard solutions, but it is necessary to assess the analytical performance of this sensor in real samples. Therefore, the constructed sensor was utilized for measurement of mephedrone in urine and plasma samples, which are biological fluids and contain a mixture of proteins and the other interfering substances. Since, there is no mephedrone consumer in Iran, we had to spike mephedrone solutions to the prepared real samples. To this end, the diluted samples were spiked with appropriate concentrations of mephedrone and the standard addition method was employed for the measurement of the prepared samples. The results obtained from these measurements, are summarized in Table 2. Inspection of the obtained results confirm the successful operation of the proposed sensor for detection of mephedrone in urine and plasma samples.

4. Conclusion

In this study, a new electrochemical imprinted sensor was developed for determination of mephedrone in solutions. The combination of sol-gel MIP, polytyramine and f-MWCNTs@AuNPs nanocomposite, results in the fabrication of an ultrasensitive and selective electrode toward the mephedrone. The proposed electrode has been overcome some shortcomings of the conventional MIP-based sensors such as weak electrochemical response, long response time and difficult preparation of the sensor. Also, the developed sensor exhibits a detection limit of 0.8 nM (142 pg ml^{-1}) and a good stability, reproducibility and repeatability. In addition, the acceptable recoveries reveal that the proposed electrochemical sensor, can be used for determination of mephedrone in biological samples in the future.

Appendix A. Supporting information

Supplementary data associated with this article can be found in the online version at doi:10.1016/j.bios.2018.08.016

References

Advisory Council on the Misuse of Drugs, 2015. Report number 454039. ⟨https://www.gov.uk/government/uploads/system/uploads/attachment_data/file/454039/Definitions_report_final_14_august.pdf⟩ (last Accessed date 5 January 2016).
Afkhami, A., Bahiraei, A., Madrakian, T., 2016. Mat. Sci. Eng. C 59, 168–176.
Amaratunga, P., Lemberg, B.L., Lemberg, D., 2013. J. Anal. Toxicol. 37, 622–628.
Bagheri, H., Hajian, A., Rezaei, M., Shirzadmehr, A., 2017. J. Hazard. Mater. 324, 762–772.
Banks, C.E., Compton, R.G., 2006. Analyst 131, 15–21.

Banks, C.E., Davies, T.J., Wildgoose, G.G., Compton, R.G., 2005. Chem. Commun. 7, 829–841.

Deiminiat, B., Rounaghi, G.H., Arbab-Zavar, M.H., 2017a. Sens. Actuators B 238, 651–659.

Deiminiat, B., Rounaghi, G.H., Arbab-Zavar, M.H., Razavipanah, I., 2017b. Sens. Actuators B 242, 158–166.

Deiminiat, B., Razavipanah, I., Rounaghi, G.H., Arbab-Zavar, M.H., 2017c. Sens. Actuators B 244, 785–795.

Donkova, B., Vasileva, P., Nihtianova, D., Velichkova, N., Stefanov, P., Mehandjiev, D., 2011. J. Mater. Sci. 46, 7134–7143.

Gao, G., Guo, D., Wang, C., Li, H., 2007. Electrochem. Commun. 9, 1582–1586.

Hamidi, H., Bozorgzadeh, S., Haghighi, B., 2017. Microchim. Acta 184, 4537–4543.

Haupt, K., Mosbach, K., 2000. Chem. Rev. 100, 2495–2504.

Jankovics, P., Varadi, A., Tolgyesi, L., Lohner, S., Nemeth-Palotas, J., Koszegi-Szalai, H., 2011. Forensic Sci. Int. 210, 213–220.

Johnson, R.D., Botch-Jones, S.R., 2013. J. Anal. Toxicol. 37, 51–55.

Li, Y., Song, H., Zhang, L., Zuo, P., Ye, B.-C., Yao, J., Chen, W., 2016. Biosens. Bioelectron. 78, 308–314.

Li, X., Uboh, C.E., Soma, L.R., Liu, Y., Guan, F., Aurand, C.R., Bell, D.S., You, Y., Chen, J., Maylin, G.A., 2014. Rapid Commun. Mass Spectrom. 28, 217–229.

Lian, W., Liu, S., Yu, J., Li, J., Cui, M., Xu, W., Huang, J., 2013. Biosens. Bioelectron. 44, 70–76.

Lua, I.A., Lin, S.L., Lin, H.R., Lua, A.C., 2012. J. Anal. Toxicol. 36, 575–581.

Mabbott, S., Correa, E., Cowcher, D.P., Allwood, J.W., Goodacre, R., 2013. Anal. Chem. 85, 923–931.

Madrakian, T., Haghshenas, E., Ahmadi, M., Afkhami, A., 2015. Biosens. Bioelectron. 68, 712–718.

Mercolini, L., Protti, M., Catapano, M.C., Rudge, J., Sberna, A.E., 2016. J. Pharm. Biomed. Anal. 123, 186–194.

Meyer, M.R., Wilhelm, J., Peters, F.T., Maurer, H.H., 2010. Anal. Bioanal. Chem. 397, 1225–1233.

Miscoria, S.A., Barrera, G.D., Rivas, G.A., 2006. Sens. Actuators B 115, 205–211.

Mohamed, R., Richoz-Payot, J., Gremaud, E., Mottier, P., Yilmaz, E., Tabet, J.C., Guy, P.A., 2007. Anal. Chem. 79, 9557–9565.

Prasad, B.B., Singh, R., 2015. Sens. Actuators B 212, 155–164.

Qiu, Z., Shu, J., Tang, D., 2018. Anal. Chem. 90, 1021–1028.

Rezaei, B., Khalili Boroujeni, M., Ensafi, A.A., 2014. Biosens. Bioelectron. 60, 77–83.

Santali, E.Y., Cadogan, A.K., Daeid, N.N., Savage, K.A., Sutcliffe, O.B., 2011. J. Pharm. Biomed. Anal. 56, 246–255.

Shen, A., Guo, J., Xie, W., Sun, M., Richards, R., Hu, J., 2011. J. Raman Spectrosc. 42, 879–884.

Shu, J., Tang, D., 2017. Chem. Asian J. 12, 2780–2789.

Situmorang, M., Gooding, J.J., Hibbert, D.B., Barnet, D., 1998. Biosens. Bioelectron. 13, 953–962.

Smith, J.P., Metters, J.P., Irving, C., Sutcliffe, O.B., Banks, C.E., 2014. Analyst 139, 389–400.

Sun, Y., Du, H., Lan, Y., Wang, W., Liang, Y., Feng, C., Yang, M., 2016. Biosens. Bioelectron. 77, 894–900.

Tan, F., Smith, J.P., Sutcliffe, O.B., Banks, C.E., 2015. Anal. Methods 7, 6470–6474.

Torrance, H., Cooper, G., 2010. Forensic Sci. Int. 202, E62–E63.

Tran, L.D., Piro, B., Pham, M.C., Ledoan, T., Angiari, C., Dao, L.H., Teston, F., 2003. Synth. Met. 139, 251–262.

Wang, J.F., Cormack, P.A.G., Sherrington, D.C., Khoshdel, E., 2003. Angew. Chem. Int. Ed. 42, 5336–5338.

Wood, D.M., Greene, S.L., Dargan, P.I., 2011. Emerg. Med. J. 28, 280–282.

Wu, Z.S., Li, J.S., Deng, T., Luo, M.H., Shen, G.L., Yu, R.Q., 2005. Anal. Biochem. 337, 308–315.

Xiao, L., Wildgoose, G.G., Compton, R.G., 2009. Sens. Actuators B 138, 524–531.

Yang, Y., Fang, G., Liu, G., Pan, M., Wang, X., Kong, L., He, X., Wang, S., 2013. Biosens. Bioelectron. 47, 475–481.

Yuan, L., Zhang, J., Zhou, P., Chen, J., Wang, R., Wen, T., Li, Y., Zhou, X., Jiang, H., 2011. Biosens. Bioelectron. 29, 29–33.

Zhang, K., Lv, S., Lin, Z., Li, M., Tang, D., 2018. Biosens. Bioelectron. 101, 159–166.

Zhang, K., Lv, S., Lin, Z., Tang, D., 2017. Biosens. Bioelectron. 95, 34–40.

Zhang, J., Niu, Y., Li, S., Luo, R., Wang, C., 2014. Sens. Actuators B 193, 844–850.

Zhao, M., Sun, L., Crooks, R.M., 1998. J. Am. Chem. Soc. 120, 4877–4878.

Zhou, Q., Lin, Y., Zhang, K., Li, M., Tang, D., 2018. Biosens. Bioelectron. 101, 146–152.

Zuway, K.Y., Smith, J.P., Foster, C.W., Kapur, N., Banks, C.E., Sutcliffe, O.B., 2015. Analyst 140, 6283–6294.